



## Resonance characteristics of tides in branching channels

Niels C. Alebregtse<sup>1,†</sup>, H. E. de Swart<sup>1</sup> and H. M. Schuttelaars<sup>2</sup>

<sup>1</sup>Institute for Marine and Atmospheric research Utrecht, Utrecht University, Princetonplein 5, 3584CC Utrecht, The Netherlands

<sup>2</sup>Delft Institute of Applied Mathematics/Mathematical Physics, Delft University of Technology, Mekelweg 4, P.O.Box 5031, 2600 GA Delft, The Netherlands

(Received 1 February 2013; revised 11 May 2013; accepted 18 June 2013; first published online 9 July 2013)

Resonance characteristics of tidal waves in a network are investigated with the linearized, one-dimensional shallow water equations. The network comprises a semi-enclosed main channel with an adjacent secondary channel at an arbitrary position. Water motion is forced by a prescribed incoming wave at the entrance of the main channel. The model is used to compute the ratio of sea surface height amplitude in the presence and absence of the secondary channel. Relevance lies in the possible construction of secondary channels to reduce tidal range in the main channel. When  $\mu = 2\pi l_b^*/l_t^* \gtrsim \pi$  ( $l_b^*$  being the length of the main channel,  $l_t^*$  the tidal wavelength) and friction is weak, it is found that reduction (amplification) of the tidal range occurs for secondary channels located less (more) than a quarter wavelength from the closed end of the main channel. Furthermore, a minimum is observed halfway between the closed end and the nodal point, and a maximum a quarter wavelength further seaward. With increasing friction and/or decreasing length of the main channel, amplitude ratios become less pronounced and depend weakly on the location of the secondary channel. The mechanism responsible for amplification or reduction of the sea surface height in the main channel is identified and explained in terms of the forced wave and waves radiating away from the secondary channel.

**Key words:** coastal engineering, shallow water flows, surface gravity waves

### 1. Introduction

Tidal embayments and estuaries are often subject to human interventions. Knowledge of the influence of such interventions on tidal hydrodynamics is important for safety regulations and ecology in these areas. Therefore, theoretical model studies have been performed to assess the response of tidal characteristics in an embayment to, amongst others, changes in its length (Prandle & Rahman 1980; Schuttelaars &

<sup>†</sup> Email address for correspondence: [n.c.alebregtse@uu.nl](mailto:n.c.alebregtse@uu.nl)

de Swart 2000; Rainey 2009; Schuttelaars, de Jonge & Chernetsky 2013) and depth (Chernetsky, Schuttelaars & Talke 2010).

Changes of tidal characteristics in embayments may also be induced by the presence of harbours or secondary channels along their sides. Construction of secondary channels is currently being considered by coastal managers to reduce negative effects of previous interventions, such as increased tidal range (Donner *et al.* 2012). So far, studies on harbours have mostly been limited to research on free modes (Defant 1961) and resonance characteristics (Miles 1971; de Jong & Battjes 2004). How secondary channels influence the water motion in their surrounding areas is less well known. This phenomenon, related to radiation damping, has been investigated in coastal dynamics by, amongst others, Buchwald (1971), Garrett (1975), Zimmerman (1992) and Mei, Stiassnie & Yue (2005). These studies assumed that the forcing wave, which is present in the absence of a secondary channel, occurred in a semi-unbounded domain.

The problem introduced here has an analogy in acoustics, where uniform pipes are considered with side branches, which can act as acoustic filters (cf. Lighthill 1978; Kinsler *et al.* 2000). There, the side branches are closed at one end, but both ends of the main pipe are open, thus preventing any reflection of the radiated waves.

The novel aspect of this work is that changes of tidal wave characteristics will be determined in a main channel, which is closed at one end, due to the presence of a secondary channel including friction. Specifically, the effect of secondary channel characteristics (location, length, depth, shape) on the amplification of incoming waves in the main channel will be assessed. Here, amplification is defined as the ratio of the sea surface height amplitude in the presence and absence of the secondary channel. To that end, § 2 will describe the model set-up. Results will be presented in § 3, and will be discussed in § 4. Finally, conclusions are presented in § 5.

## 2. Model and methods

A model is considered that solves the hydrodynamics in a channel network. The network consists of a main channel with length  $l_b^*$ , and a secondary channel located at a distance  $x_{sc}^*$  from the open boundary. The main channel is split into two parts: channel 1 is located seaward of the secondary channel and channel 2 landward. The secondary channel is called channel 3. The width, depth and friction of the channels in the network are constant throughout each channel, but can vary among them (see figure 1).

The one-dimensional, linearized shallow water equations describe the water motion in the network. These are the along-channel momentum balance and the continuity equations,

$$\frac{\partial u_j^*}{\partial t^*} = -g^* \frac{\partial \eta_j^*}{\partial x_j^*} - \frac{\lambda_j^* u_j^*}{h_j^*}, \quad (2.1)$$

$$\frac{\partial \eta_j^*}{\partial t^*} = -h_j^* \frac{\partial u_j^*}{\partial x_j^*}. \quad (2.2)$$

Here, the symbol \* indicates a dimensional quantity,  $j$  is the channel index,  $u_j^*$  ( $x_j^*$ ) the velocity (coordinate) along the main axis of each channel,  $\eta_j^*$  the sea surface elevation,  $t^*$  the time,  $g^*$  the acceleration due to gravity,  $\lambda_j^*$  the dimensional linear friction coefficient, and  $h_j^*$  the depth. Finally,  $w_j^*$  is the width of channel  $j$ , which will appear when applying mass continuity at the vertex point.

## Tidal resonance in branching channels

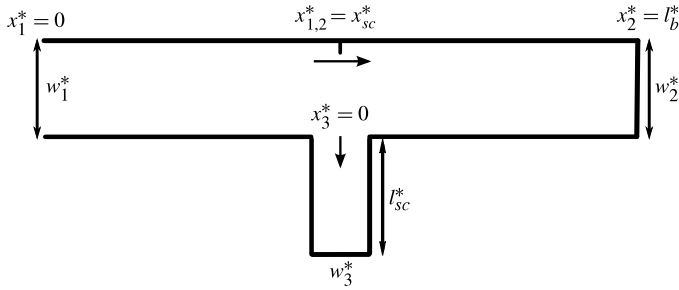


FIGURE 1. Model domain consisting of a main channel with length  $l_b^*$  and a secondary channel with length  $l_{sc}^*$  at distance  $x_{sc}^*$  from the open boundary. The open boundary is at  $x_1^* = 0$ , where an incoming wave is prescribed. The channel widths are  $w_j^*$  ( $j = 1, 2, 3$ ) and  $x_j^*$  is the along-axial coordinate.

Six boundary conditions have to be prescribed for (2.1) and (2.2), two for each branch of the network. The general approach to obtain the condition at the open boundary  $x^* = 0$  is to derive the Green's function for the outer domain  $x^* < 0$  (cf. Garrett 1975). Here, a simpler condition is imposed, which is done for analytical tractability. This condition consists of a sea surface amplitude forcing by an incoming tidal wave with angular frequency  $\sigma^* = 2\pi/T^*$ , where  $T^*$  is the tidal period (typically,  $T^*$  is 12 h 25 min for the  $M_2$  tide). It is assumed that the incoming wave remains unchanged under changing conditions in the network, and changes of the incoming wave, e.g. due to (partial) reflection of the outgoing wave outside the domain, are assumed negligible. The present approach differs from prescribing a fixed amplitude at the open boundary, which is observed in co-oscillating basins, in that the latter model keeps the sum of the incoming and reflected wave fixed. The landward boundaries of the main channel and of the secondary channel are closed. Finally, matching conditions connect the channels at the vertex point. These are continuity of sea surface elevation (twice) and conservation of mass.

Equations (2.1) and (2.2) are made dimensionless, by introducing

$$u_j^* = U^* u_j, \quad x_j^* = l_b^* x_j, \quad w_j^* = w_1^* w_j, \quad (2.3a)$$

$$\eta_j^* = N^* \eta_j, \quad t^* = t/\sigma^*, \quad h_j^* = h_1^* h_j. \quad (2.3b)$$

Here,  $U^* = N^* l_b^* \sigma^* / h_1^*$  is a typical velocity scale (following from continuity) and  $N^*$  is the amplitude of the incoming wave. Applying these scales to the dimensional equations results in

$$\frac{\partial u_j}{\partial t} = -\frac{1}{\mu^2} \frac{\partial \eta_j}{\partial x_j} - \frac{\lambda_j u_j}{h_j}, \quad (2.4)$$

$$\frac{\partial \eta_j}{\partial t} = -h_j \frac{\partial u_j}{\partial x_j}, \quad (2.5)$$

where  $\mu = 2\pi l_b^* / l_t^*$  is, apart from a factor  $2\pi$ , the ratio of the length of the main channel and the tidal wavelength ( $l_t^* = \sqrt{g^* h_1^* T^*}$ ) and  $\lambda_j = \lambda_j^* / (h_1^* \sigma^*)$  is the dimensionless linear friction coefficient.

Equations (2.4) and (2.5) can be combined into wave equations for the free surface in each channel. Their solutions are of the form  $(\eta_j(x, t), u_j(x, t)) = (\hat{\eta}_j(x), \hat{u}_j(x))e^{-it} + \text{c.c.}$ , where the hat  $\hat{\phantom{x}}$  indicates a complex amplitude and c.c. denotes a complex

conjugate. The resulting equation for the complex sea surface amplitudes  $\hat{\eta}_j$  is

$$\frac{d^2 \hat{\eta}_j}{dx_j^2} + \frac{\mu^2}{h_j} \left( 1 + i \frac{\lambda_j}{h_j} \right) \hat{\eta}_j = 0, \quad (2.6)$$

which has solutions of the form

$$\hat{\eta}_j = A_{j,1} e^{i\kappa_j x_j} + A_{j,2} e^{-i\kappa_j x_j}, \quad j = 1, 2, 3, \quad (2.7)$$

with  $\kappa_j = (\mu/h_j) \sqrt{h_j + i\lambda_j}$  the complex wavenumber. The first term on the right-hand side denotes the spatial part of a wave propagating in the  $+x$ -direction (incoming), whereas the second term denotes the spatial part of a wave propagating in the  $-x$ -direction (outgoing).

The boundary conditions for (2.7) are mathematically given as

$$A_{1,1} = 1 \quad \text{at } x_1 = 0, \quad (2.8)$$

$$\hat{u}_2 = 0 \quad \text{at } x_2 = 1, \quad (2.9)$$

$$\hat{u}_3 = 0 \quad \text{at } x_3 = \tilde{l}, \quad (2.10)$$

$$\hat{\eta}_1 = \hat{\eta}_2 \quad \text{at } x_1 = x_2 = x_{sc}, \quad (2.11)$$

$$\hat{\eta}_1 = \hat{\eta}_3 \quad \text{at } x_1 = x_{sc}, x_3 = 0, \quad (2.12)$$

$$\hat{u}_1 = w_2 h_2 \hat{u}_2 + w_3 h_3 \hat{u}_3 \quad \text{at } x_1 = x_2 = x_{sc}, x_3 = 0, \quad (2.13)$$

where  $\tilde{l} = l_{sc*}/l_{b*}$  is the dimensionless length of the secondary channel.

### 3. Results

#### 3.1. Model solutions

For the remainder of the analysis, it will be assumed that the width and depth of the main channel are the same in channels 1 and 2. This results in equal wavenumbers in both areas, thereby simplifying the analysis. The solutions of system (2.6)–(2.13) are

$$\hat{\eta}_1(x_1) = \frac{2e^{i\kappa_1 x_{sc}}}{(1 - i\alpha)} [\cos(\kappa_1(x_1 - x_{sc})) + \alpha \sin(\kappa_1(x_1 - x_{sc}))], \quad 0 \leq x_1 \leq x_{sc}, \quad (3.1)$$

$$\hat{\eta}_2(x_2) = \frac{2e^{i\kappa_1 x_{sc}} \cos(\kappa_1(1 - x_2))}{(1 - i\alpha) \cos(\kappa_1(1 - x_{sc}))}, \quad x_{sc} \leq x_2 \leq 1, \quad (3.2)$$

$$\hat{\eta}_3(x_3) = \frac{2e^{i\kappa_1 x_{sc}} \cos(\kappa_3(\tilde{l} - x_3))}{(1 - i\alpha) \cos(\kappa_3 \tilde{l})}, \quad 0 \leq x_3 \leq \tilde{l}, \quad (3.3)$$

where

$$\alpha = \tan(\kappa_1(1 - x_{sc})) + w_3 \frac{\kappa_1}{\kappa_3} \tan(\kappa_3 \tilde{l}). \quad (3.4)$$

Now, the complex amplitude ratio,  $CAR \equiv A_r e^{i\delta}$ , of the wave is computed as the ratio of the wave amplitude in the presence and absence of the secondary channel. The latter situation, identical to a single channel, is computed by using (3.1)–(3.4) with  $\tilde{l} = 0$ . Note that this implies separate solutions of the complex amplitude ratio for stretches 1 and 2 of the main channel, indicated as  $CAR^{(1)}$  and  $CAR^{(2)}$ . The results are

$$CAR^{(1)} = \frac{e^{i\kappa_1(x_{sc}-1)}}{(1 - i\alpha)} \left[ \frac{\cos(\kappa_1(x_1 - x_{sc})) + \alpha \sin(\kappa_1(x_1 - x_{sc}))}{\cos(\kappa_1(x_1 - 1))} \right] \equiv A_r^{(1)} e^{i\delta^{(1)}}, \quad (3.5)$$

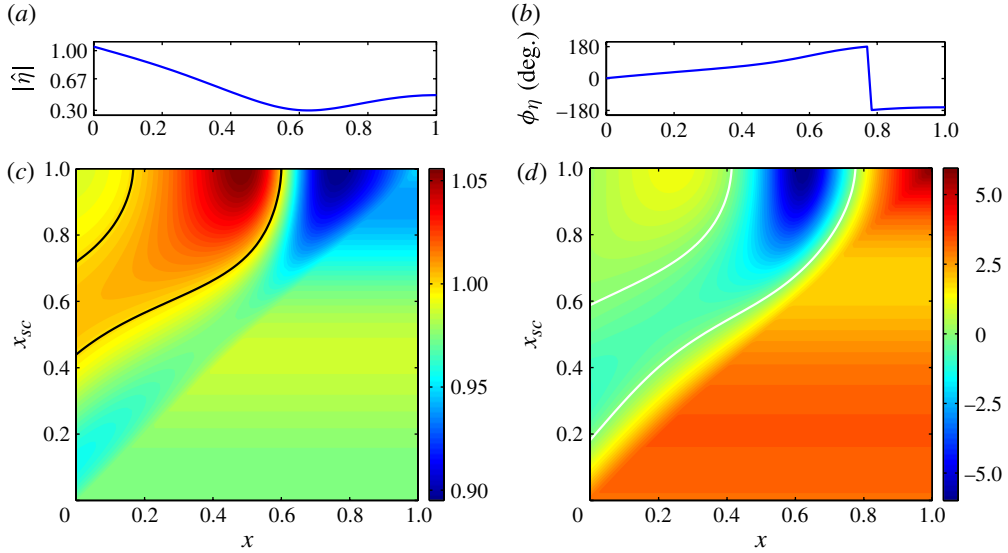


FIGURE 2. Sea surface height characteristics in the main channel for the default case. (a) The amplitude in the absence of a secondary channel as a function of distance  $x$  to the open boundary. (b) The phase of the sea surface height,  $\phi_\eta$ , in the absence of the secondary channel. (c) The amplitude ratio  $A_r$  as a function of  $x$  and location  $x_{sc}$  of the secondary channel. (d) The phase difference,  $\delta$ , between the free surface with and without the secondary channel as a function of  $x$  and  $x_{sc}$ .

$$\text{CAR}^{(2)} = \frac{e^{i\kappa_1(x_{sc}-1)}}{(1-i\alpha)\cos(\kappa_1(x_{sc}-1))} \equiv A_r^{(2)} e^{i\delta^{(2)}}. \quad (3.6)$$

Note that  $\text{CAR}^{(2)}$  is independent of  $x_2$ , which will be explained in § 4.

Equations (3.4), (3.5) and (3.6) reveal that tidal amplification is controlled by three parameters, i.e.  $x_{sc}$ ,  $\kappa_1$ , and

$$S_f = \frac{w_3}{\kappa_3} \tan(\kappa_3 \tilde{l}). \quad (3.7)$$

Parameter  $S_f$ , which appears in parameter  $\alpha$ , will be called the secondary channel factor and contains all the information on the dimensions of the secondary channel.

### 3.2. Default system

As a default system, a network is defined having all parameter values equal to 1, with the exception of  $\mu$ , which is equal to  $\pi$ , and  $\mu\tilde{l}$ , which is 0.1. These parameters represent estuaries of intermediate dimensions, such as Chesapeake Bay on the east coast of the United States. Zhong, Li & Foreman (2008) showed that tides in the Chesapeake Bay are partially standing, and that friction is weak to moderate. Moreover this choice ensures that the full dynamics of the mechanism is captured.

Figures 2(a) and 2(b) show the amplitude and phase of the sea surface height,  $|\hat{\eta}|$  and  $\phi_\eta$  respectively, in the main channel for the default case without a secondary channel. Both panels show the partial standing character of the tidal wave. Figures 2(c) and 2(d) show the amplitude ratio and phase shift for the default system,  $A_r$  and  $\delta$  respectively, in the main channel. Parameter  $\delta$  represents the phase shift between the tides in the presence and absence of the secondary channel.

Figure 2(c) shows the amplitude ratio as a function of  $x$  and  $x_{sc}$ . The solid black line is the unit contour, separating areas in  $(x, x_{sc})$ -parameter space where  $A_r > 1$  from those where  $A_r < 1$ . Note that a minimum in the amplitude ratio is observed around  $x_{sc} = 0.92$ . The amplitude ratio  $A_r^{(2)} < 1$ , indicating a decrease in sea surface height amplitude throughout channel 2 for all locations of the secondary channel. However, in channel 1 values of  $A_r^{(1)}$  larger than 1 are observed, hence locally the tide can be amplified. Finally, near  $x = 0$  it is found that  $A_r \neq 1$ , meaning that the secondary channel influences the tidal characteristics at the open boundary. This occurs mainly when the secondary channel is positioned close to the open boundary. The effect becomes smaller when the distance between the open boundary and the secondary channel increases and friction causes dampening of the perturbation of the intervention.

Figure 2(d) shows the phase shift,  $\delta$ , caused by the secondary channel as a function of  $x$  and  $x_{sc}$ , where solid white lines are the zero contours. This figure shows that the presence of the secondary channel influences the time of high and low water. This signal is approximately  $90^\circ$  out of phase with the amplitude ratio.

### 3.3. Sensitivity analysis

As a next step, the sensitivity of  $A_r^{(2)}$  to  $S_f$ ,  $\kappa_1$ , and  $x_{sc}$  will be investigated. This is done because from a management perspective often the tidal range at the head of the estuary is of importance (Donner *et al.* 2012). Changing  $S_f$  is equivalent to changing the secondary channel characteristics: width  $w_3$ , length  $\tilde{l}$ , depth  $h_3$ , and friction coefficient  $\lambda_3$ . Variation in  $\kappa_1$  is achieved by changing the length ( $\mu$ ) of the main channel and the friction parameter ( $\lambda_{1,2,3}$ ) in the entire network. Finally, changing  $x_{sc}$  shifts the position of the secondary channel.

The sensitivity of the amplitude ratio to  $S_f$  is shown in figure 3(a) for a secondary channel located halfway along the main channel. The real part of  $S_f$  is along the horizontal axis and the imaginary part of  $S_f$  is along the vertical axis. Colours represent different values of  $A_r^{(2)}$ . The solid white line indicates the unit contour level.

First, the circles in the figure represent the values of  $S_f$  for all parameters having their default values, except that the length of the secondary channel is varied. Each circle indicates an increment of 0.3 in the direction of the arrow, starting at the origin with  $\tilde{l} = 0$ . Figure 3(b) shows the value of  $A_r^{(2)}$  when following the circles, indicating that for large  $\tilde{l}$  the amplitude ratio is a constant. This occurs because the reflected wave is damped in the secondary channel. Indeed, from (3.7) it can be seen that for  $\tilde{l}$  approaching infinity, the secondary channel factor goes to a constant value of  $iw_3/\kappa_3$ , which is shown by the white dashed line in figure 3(a). Increasing the width results in smaller amplitude ratios.

Second, the crosses indicate the functional behaviour of  $S_f$  with varying  $h_3$ , starting with zero depth at the origin. Again, symbols denote increments of 0.3 in the direction of the arrow. As  $h_3$  becomes large  $\kappa_3$  approaches zero. Then from (3.7) it is seen that  $\tan(\kappa_3\tilde{l}) \sim \kappa_3\tilde{l}$ , resulting in a constant real secondary channel factor of  $w_3\tilde{l}$ .

Finally, the plusses in figure 3(a) show  $S_f$  as a function of  $\lambda_3$ . For a frictionless system,  $\lambda_3 = 0$ , the secondary channel factor is a real number since  $\text{Im}(\kappa_3) = 0$ . For large  $\lambda_3$ , friction is so strong that it prevents wave propagation into the secondary channel, thereby resulting in no modification of the original wave.

Next,  $A_r^{(2)}$  is computed for different lengths of the main channel, different friction values throughout the network, and different positions of the secondary channel. The

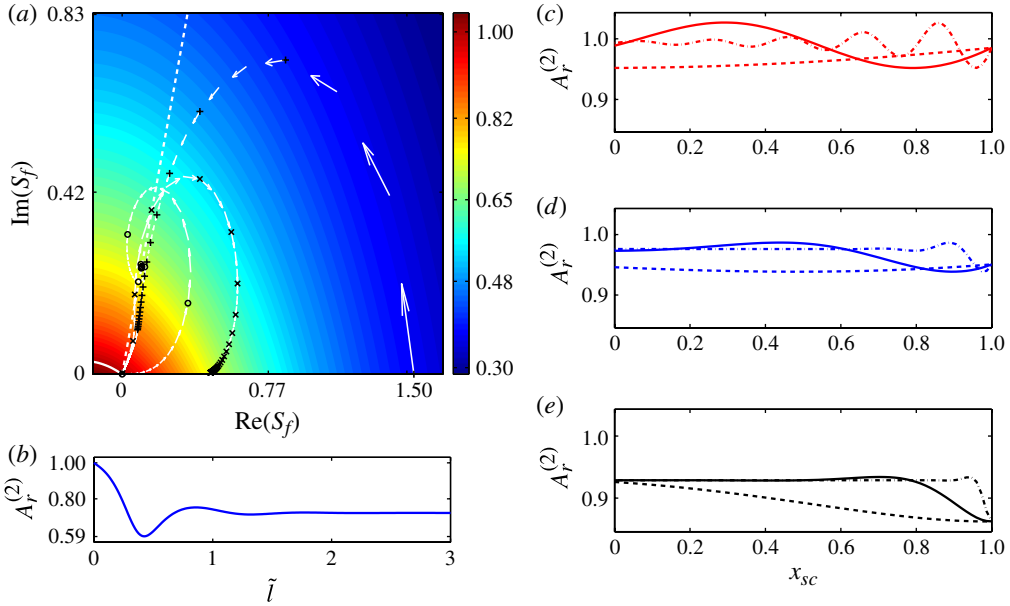


FIGURE 3. (a) Colour plot of the amplitude ratio  $A_r^{(2)}$  in channel 2 for  $x_{sc} = 0.5$  as a function of the real and imaginary part of the secondary channel factor  $S_f$ , defined in (3.7). The circles show the behaviour of  $S_f$  for varying length  $\tilde{l}$  of the secondary channel, the crosses for varying depth  $h_3$ , and the pluses for varying friction coefficient  $\lambda_3$ . All markers indicate increments of 0.3 in the respective variable, directed along the arrows. (b)  $A_r^{(2)}$  as a function of  $\tilde{l}$  when following the circles. The white dashed line in (a) shows the limit as  $\tilde{l}$  becomes large of the circles for different widths of the secondary channel. (c,d,e)  $A_r^{(2)}$  for different  $\mu$  and  $\lambda$  as a function of  $x_{sc}$ : the solid line represents  $\mu = \pi$ , the dashed line  $\mu = \pi/5$ , and the dashed-dotted line  $\mu = 5\pi$ ; (c)  $\lambda_j = 1/5$  (weak friction), (d)  $\lambda_j = 1$  (moderate friction), and (e)  $\lambda_j = 5$  (strong friction).

results are presented in figure 3(c,d,e). The solid line represents the results for the default main channel length, while the dashed (dashed-dotted) line represents those for the case that the length of the main channel is decreased (increased) by a factor of five. Figure 3(d) shows results for the default value of the friction coefficient, while figure 3(c) (figure 3e) shows those for decreased (increased) friction by a factor five in the entire network.

Increasing friction mainly results in a decreasing value and spatial dependence of the amplitude ratio. A striking feature is observed for the default channel length with low friction (red solid line). Here, reduction of the amplitude is observed for secondary channel locations from  $0.5 \leq x_{sc} \leq 1$ , while amplification is observed for locations ranging from  $0 \leq x_{sc} \leq 0.5$ . Increasing friction results in a decrease of the amplitude ratio, finally leading to the vanishing of positions for which amplification is found.

## 4. Discussion

### 4.1. Physical mechanism

First, the mechanism will be discussed that causes the differences in amplitude and phase of the tidal wave in the main channel due to the presence of the secondary channel. The situation sketch in figure 4(a) shows the incoming waves (solid arrows)

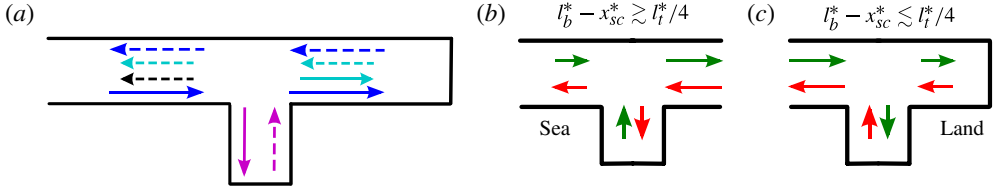


FIGURE 4. (a) Incoming (solid arrows) and outgoing (dashed arrows) waves in the domain. For definition of colours see the text. (b) Flood (green arrows) and ebb (red arrows) velocities around the secondary channel located close to the nodal point of the forcing wave. For locations seaward of the nodal point mass is extracted from the secondary channel during flood. (c) As (b) but for a secondary channel located landward of the nodal point. Now, mass is extracted from the secondary channel during ebb.

and outgoing waves (dashed arrows) in all channels. The forcing at the open boundary generates a primary wave (blue arrow) that propagates into the channel. At the vertex point it triggers a partially standing wave (purple arrows) in the secondary channel. The latter leads to two secondary (radiated) waves in the main channel, one incoming and one outgoing (cyan solid and black dashed arrows, respectively). The incoming primary wave (which, by definition, is unaffected by the secondary channel) and the incoming radiated wave reflect at the landward boundary. The resulting outgoing waves additionally affect the partially standing wave in the secondary channel.

The complex amplitude ratio in channel 2,  $CAR^{(2)}$ , is determined for every  $x$  by the ratio of the complex amplitude  $A_{2,1}$  of the incoming wave at the vertex point in the presence, and in the absence, of the secondary channel. Furthermore, it is a constant because the incoming waves in channel 2 experience identical friction regardless of the presence of a secondary channel. According to (2.7), (2.8) and (3.1), the amplitude of the incoming primary wave at the vertex point can be written as  $\exp(i\kappa_1 x_{sc})$ . Thus, the complex amplitude ratio is

$$CAR^{(2)} = 1 + A_{rad} e^{-i\kappa_1 x_{sc}}. \quad (4.1)$$

By combining (2.10), (2.11) and (2.13), the amplitude of the incoming radiated wave at the vertex point can be written in terms of the amplitude of the outgoing wave at the vertex point from the side channel as

$$A_{rad} = \frac{w_3 \kappa_1}{2\kappa_3} (1 - e^{-2i\kappa_3 \tilde{l}}) A_{3,2}, \quad (4.2)$$

which for a short secondary channel ( $\mu \tilde{l} \ll 1$ ) simplifies to

$$A_{rad} \approx iw_3 \kappa_1 \tilde{l} A_{3,2}. \quad (4.3)$$

Furthermore, the combination of (2.9)–(2.12) yields, for the amplitude of the outgoing wave in the secondary channel at the vertex point,

$$A_{3,2} = \frac{1 + e^{2i\kappa_1(1-x_{sc})}}{1 + e^{-2i\kappa_3 \tilde{l}}} (e^{i\kappa_1 x_{sc}} + A_{rad}). \quad (4.4)$$

Again assuming  $\mu \tilde{l} \ll 1$  and using (4.3), this can be approximated as

$$A_{3,2} \approx \frac{1}{2} (1 + e^{2i\kappa_1(1-x_{sc})}) e^{i\kappa_1 x_{sc}}. \quad (4.5)$$

### *Tidal resonance in branching channels*

By substituting (4.3) and (4.5) into (4.1), the solution for the complex amplitude ratio becomes

$$\text{CAR}^{(2)} \approx 1 + iw_3\kappa_1\tilde{l}\cos(\kappa_1(1-x_{sc}))e^{i\kappa_1(1-x_{sc})}. \quad (4.6)$$

Next, the low friction limit ( $\text{Im}(\kappa_j) = 0$ ) is considered, as it yields considerable insight into the modifying mechanism of the tide due to the secondary channel. The amplitude ratio in this limit is

$$A_r^{(2)} \approx [1 - w_3\kappa_1\tilde{l}\sin(2\kappa_1(1-x_{sc}))]^{1/2}. \quad (4.7)$$

Now, tidal range decreases ( $A_r^{(2)} < 1$ ) when  $\sin(2\kappa_1(1-x_{sc})) > 0$ , while tidal range increases when  $\sin(2\kappa_1(1-x_{sc})) < 0$ . Thus, positions of the secondary channel resulting in smaller tidal ranges are those for which the secondary channel is located less than a quarter wavelength away from the closed end of the main channel, i.e.  $0 \leq \kappa_1(1-x_{sc}) \leq \pi/2$ , modulo  $\pi$ . Amplification occurs for  $\pi/2 \leq \kappa_1(1-x_{sc}) \leq \pi$ , modulo  $\pi$ . The minimum (maximum) amplitude ratio is observed at 1/8 times the wavelength of the tidal wave seaward from the open end (nodal point), since the radiated wave is strongest when both sea surface height amplitude and velocities are large.

The amplification is caused by the fact that, if the secondary channel is located more than a quarter wavelength from the closed end (figure 4*b*), it discharges its water into the main channel during flood tides. This is because the maximum velocity amplitude is attained at the nodal point of the primary wave. Consequently, velocities are smaller in front of the secondary channel than behind it when the secondary channel is located seaward from the nodal point. When the secondary channel is located landward from the nodal point the reverse processes occur, causing the secondary channel to discharge water in the main channel during ebb, leading to reduction of the tidal range in channel 2 (figure 4*c*).

#### *4.2. Relevance and limitations*

This study has yielded fundamental insight into the mechanisms dominating the response of channel networks to changes in network geometry, which has important implications for engineering works, where man-made secondary channels are being considered as a measure to reduce tidal range in estuaries, e.g. in the Ems estuary situated at the Dutch–German border.

It was shown that for short secondary channels the amplitude of the modulating tidal wave was small ( $O(\mu\tilde{l})$ ) compared to that of the forced incoming wave. Therefore, adding an additional secondary channel to the system leads to a linear addition of its effect, since the response of the interaction between the secondary channels and the main channel is  $O((\mu\tilde{l})^2)$ .

The chosen representation of the system is obviously simplified. However, results with a sloping bottom in the main channel indicate that for realistic bottom slopes, i.e. a decrease in depth of up to half the initial depth, the behaviour is qualitatively similar to that for a constant depth. Similarly, changing the secondary channel to a Helmholtz basin with a narrow inlet channel followed by a wider basin yields no qualitative changes in the model results. Moreover, the linear friction coefficient should be obtained through a linearization procedure of the quadratic bottom stress (cf. Zimmerman 1992, and references therein). The coefficient obtained by considering only the main channel might not be representative for the network, which includes a

secondary channel. Nevertheless, numerical experiments with a quadratic bottom stress show very similar results, indicating little sensitivity to the linearization procedure.

Finally, note that although this research was applied to tidal characteristics, it can also be used to compute resonance characteristics of long gravity waves in harbours.

## 5. Conclusions

This study has provided both a quantitative and qualitative assessment of the dependence of amplitude and phase of tidal waves in a semi-enclosed channel on the geometrical characteristics of a secondary channel. For this, analytical solutions of the linear one-dimensional shallow water equations, which govern the tidal motion in the network due to an imposed incoming wave at the open boundary, have been constructed and interpreted. From these an amplitude ratio has been defined as the ratio of the local amplitude of the sea surface height in the main channel in the presence and in the absence of the secondary channel.

For lengths of the main channel of the order of the tidal wavelength, short secondary channels and weak friction, it has been found that the secondary channel causes tides in the main channel to weaken (amplitude ratio  $<1$ ) if it is located between a node and the successive landward located antinode of the tide. Conversely, if the secondary channel is located between a node and the successive seaward located antinode, it causes tides in the main channel to become more resonant. The physical mechanism underlying this behaviour is that in the former case tidal velocities in the main and secondary channel near the vertex point are in phase, so that e.g. during flood the secondary channel accommodates part of the incoming water volume. In the latter case these velocities are out of phase and thus the opposite occurs.

Results reveal that there are optimum lengths and depths of the secondary channel for which the changes in tidal resonance characteristics in the main channel are maximum. Larger widths cause the amplitude ratio to become small. Increasing friction in, and/or reducing the length of the main channel, causes the variations of the amplitude ratio to become less pronounced. These conclusions are robust with respect to mild depth variations within channels, varying the shape of the secondary channel, and the detailed formulation of bottom friction. The results obtained are of interest in the context of possible construction of retention basins in estuaries to effectively reduce tidal range.

## Acknowledgements

This work is part of the research programme NWO-ALW project 843.10.001, which is financed by the Netherlands Organisation for Scientific Research (NWO) and the Chinese Organisation for Scientific Research (NSFC).

## References

- BUCHWALD, V. T. 1971 The diffraction of tides by a narrow channel. *J. Fluid. Mech.* **46** (3), 501–511.
- CHERNETSKY, A. S., SCHUTTELAARS, H. M. & TALKE, S. A. 2010 The effect of tidal asymmetry and temporal settling lag on sediment trapping in estuaries. *Ocean Dyn.* **60**, 1219–1241.
- DEFANT, A. 1961 *Physical Oceanography*, vol. 2. Pergamon.

### *Tidal resonance in branching channels*

- DONNER, M., LADAGE, F., STOSCHEK, O. & NGUYEN, H. 2012 Methods and analysis tools for redevelopments in an estuary with high suspended sediment concentrations. In *Coastal Engineering* (ed. P. Lynett & J. McKee Smith), vol. 1, p. 55. Coastal Engineering Research Council.
- GARRETT, C. 1975 Tides in gulfs. *Deep-Sea Res.* **22**, 23–35.
- DE JONG, M. P. C. & BATTJES, J. A. 2004 Low-frequency sea waves generated by atmospheric convection cells. *J. Geophys. Res.* **109**, C01011.
- KINSLER, L. E., FREY, A. R., COPPENS, A. B. & SANDERS, J. V. 2000 *Fundamentals of Acoustics*, 4th edn. John Wiley & Sons.
- LIGHTHILL, J. 1978 *Waves in Fluids*. Cambridge University Press.
- MEI, C. C., STIASSNIE, M. & YUE, D. K. P. 2005 *Theory and Applications of Ocean Surface Waves: Linear Aspects*, Advanced Series on Ocean Engineering, vol. 23. World Scientific.
- MILES, J. W. 1971 Resonant response in harbours: an equivalent-circuit analysis. *J. Fluid. Mech.* **26** (2), 241–265.
- PRANDLE, D. & RAHMAN, M. 1980 Tidal response in estuaries. *J. Phys. Oceanogr.* **10**, 1552–1573.
- RAINEY, R. C. T. 2009 The optimum position for a tidal power barrage in Severn estuary. *J. Fluid. Mech.* **636**, 497–507.
- SCHUTTELAARS, H. M., DE JONGE, V. N. & CHERNETSKY, A. S. 2013 Improving the predictive power when modelling physical effects of human interventions in estuarine systems. *Ocean Coast. Manage.* **79**, 70–82.
- SCHUTTELAARS, H. M. & DE SWART, H. E. 2000 Multiple morphodynamic equilibria in tidal embayments. *J. Geophys. Res.* **105** (C10), 24105–24118.
- ZHONG, L., LI, M. & FOREMAN, M. G. G. 2008 Resonance and sea level variability in Chesapeake Bay. *Cont. Shelf Res.* **28**, 2565–2573.
- ZIMMERMAN, J. T. F. 1992 On the Lorentz linearization of a nonlinearly damped tidal Helmholtz oscillator. *Proc. Koninklijke Nederlandse Akademie van Wetenschappen* **95** (1), 127–145.